Int. J. Therm. Sci. (1999) 38, 384–397
© Elsevier, Paris

Heat, mass and momentum transfer of a water film flowing down a tilted plate exposed to solar irradiation

Baoyin Song, Hideo Inaba*, Akihiko Horibe, Koichi Ozaki

Department of Mechanical Engineering, Faculty of Engineering, Okayama University, Tsushimanaka 3-1-1, Okayama 700-0082, Japan

(Received 15 June 1998, accepted after revision 28 October 1998)

Abstract — This paper has investigated the heat, mass and momentum transfer of a water film falling over a tilted plate with solar radiant heating and water evaporation. A cluster of physical models which include conduction, convection with flow turbulence, diffusion, radiation and phase change was developed for predicting the characteristics of heat, mass and momentum transfer. A fully implicit control-volume finite-difference procedure was used to solve the coupling equations. The effects of various parameters on heat, mass and momentum transport were investigated. The results revealed that the gradients of temperature and the mass fraction of water vapor in the gas layer, and the wind velocity played a key role in the heat and mass transfer along the gas-water interface. The water film Reynolds number related to the film thickness and the plate tilt angle markedly exerted an influence on the eddy viscosity and the turbulent Prandtl number of the water film. The ambient atmospheric temperature only dramatically affected the interfacial sensible heat transfer. The magnitude of solar incident flux had intense influence on the water film temperature but not on the interfacial heat and mass transfers. © Elsevier, Paris.

water film / solar irradiation / momentum transport / heat and mass transfer / numerical analysis

Résumé — Transfert de chaleur, de masse et de quantité de mouvement lors de l'écoulement d'un film d'eau sur une plaque inclinée exposée à l'irradiation solaire. Cet article traite des transferts de chaleur, de masse et de quantité de mouvement lors de l'écoulement d'un film d'eau sur une plaque inclinée, soumise à un chauffage par rayonnement solaire et à une évaporation. Un ensemble de modèles physiques tenant compte de la conduction, de la convection turbulente, de la diffusion, du rayonnement et du changement de phase ont été développés dans le but de prédire les caractéristiques des trois transferts en question. Une procédure volume de contrôle/différences finies totalement implicite a été utilisée pour résoudre les équations couplées. On a analysé les effets de différents paramètres sur les transferts de chaleur, de masse et de quantité de mouvement. Les résultats révèlent que les gradients de température et de fraction massique de la vapeur d'eau dans la couche gazeuse, ainsi que la vitesse du vent jouent des rôles clés dans les transferts de chaleur et de masse le long de l'interface gaz–eau. Le nombre de Reynolds du film d'eau relié à l'épaisseur du film et à l'angle d'inclinaison de la plaque exercent une influence marquée sur la viscosité turbulente et le nombre de Prandtl turbulent du film d'eau. La température ambiante n'affecte de façon importante que le transfert interfacial de chaleur sensible. La grandeur du flux solaire incident a un impact significatif sur la température du film d'eau, mais non sur les transferts interfaciaux de chaleur et de masse. © Elsevier, Paris.

film d'eau / irradiation solaire / transfert de quantité de mouvement / transferts de chaleur et de masse / analyse numérique

Nomenclature

A^+	damping constant, 25.1	
b_n	constants in Eq. (28)	
B^+	van Driest parameter defined by Eq. (28)	
c	mass fraction of water vapor	
c_p	specific heat	$J \cdot kg^{-1} \cdot K^{-1}$
D	mass diffusivity	$m^2 \cdot s^{-1}$
f	damping factor in equation (24)	
F	local radiation flux	$W \cdot m^{-2}$
F^o	radiation flux incident on the gas–water interface	$W \cdot m^{-2}$
g	gravitational acceleration	$m \cdot s^{-2}$
h	heat transfer coefficient	$W \cdot m^{-2} \cdot K^{-1}$
h_{fg}	latent heat of vaporization	$J \cdot kg^{-1}$

* Correspondence and reprints.
inaba@en2ews1.okayama-u.ac.jp

h_l	interfacial latent heat transfer coefficient	$W \cdot m^{-2} \cdot K^{-1}$
h_m	interfacial mass transfer coefficient	$m \cdot s^{-1}$
h_s	interfacial sensible heat transfer coefficient	$W \cdot m^{-2} \cdot K^{-1}$
h_x	overall interfacial heat transfer coefficient	$W \cdot m^{-2} \cdot K^{-1}$
k	molecular thermal conductivity	$W \cdot m^{-1} \cdot K^{-1}$
L	reference length	m
m	interfacial mass flux	$kg \cdot s^{-1} \cdot m^{-2}$
M_a	molar mass of air	$kg \cdot kmol^{-1}$
M_v	molar mass of vapor	$kg \cdot kmol^{-1}$
Nu	interfacial Nusselt number, $h_x x/k_g$	
p	ambient atmospheric pressure	Pa
Pr	water film Prandtl number	
Pr_t	water film turbulent Prandtl number	
$p_{v,i}$	partial pressure of water vapor at the gas–water interface	Pa
q_l	interfacial latent heat flux in gas side	$W \cdot m^{-2}$
q_s	interfacial sensible heat flux in gas side	$W \cdot m^{-2}$
q_x	total interfacial heat flux	$W \cdot m^{-2}$
Re	water film Reynolds number, $4\Gamma/\mu_l$	
RH	atmospheric relative humidity	
R_m	universal gas constant	$J \cdot kmol^{-1} \cdot K^{-1}$
Sh	interfacial Sherwood number $(= h_m x/D)$	
T	temperature	K
u	x-direction velocity	$m \cdot s^{-1}$
u_*	shear stress velocity $(= \tau_w/\rho_l)^{1/2}$	$m \cdot s^{-1}$
v	y-direction velocity	$m \cdot s^{-1}$
x	coordinate in the axial direction	m
X	dimensionless coordinate in the axial direction x/L	
y	coordinate in the transverse direction	m
Y	dimensionless coordinate in the transverse direction, y/δ_l	
y_c	the intersecting point of two eddy diffusivity models	m
y^+	dimensionless wall coordinate $y u_*/\nu$	

Greek symbols

α^*	absorptivity of surface	
β	extinction coefficient	m^{-1}
γ	inter-reflection parameter defined by equation (23)	
λ	wavelength	μm
λ_c	cutoff wavelength beyond which water is opaque to radiation	μm
ρ	density	$kg \cdot m^{-3}$
ρ^*	reflectivity of surface	
δ_l	water film thickness	m
δ_g	thickness of velocity boundary layer of gas	m
ε_m	water eddy diffusivity for momentum	$m^2 \cdot s^{-1}$
μ	dynamic viscosity	$kg \cdot m^{-1} \cdot s^{-1}$
ν	kinematic viscosity	$m^2 \cdot s^{-1}$
τ	shear stress	Pa
τ^*	transmissivity of the gas–water interface	
Γ	water mass flow rate per unit width	$kg \cdot m^{-1} \cdot s^{-1}$
ψ	tilt angle of the absorbing plate	°

Subscripts

a	dry air
av	average
g	gas mixture of dry air and water vapor
i	condition at the gas–water interface
l	liquid water
max	maximum
t	turbulent
v	vapor
w	condition at the absorbing surface
λ	condition at the wavelength of λ
o	inlet condition
∞	refers to atmosphere

Superscripts

+	refers to the forward direction
−	refers to the backward direction

1. INTRODUCTION

Liquid film flowing down a solid surface is encountered everywhere. Sweat falling down the body skin, rain falling over roofs and liquid metal flowing down a solid surface are just some examples. A gas–liquid flow system is widely employed in air conditioning, film cooling, film heating, gas absorption, humidification, solar energy collection, solar regeneration, etc.

Heat and mass transfer occurs simultaneously in gas–liquid flow systems, which have been studied by many investigators [1–9]. Among them, Yan and Soong [1] investigated forced convective heat and mass transfer along an inclined heated plate with film evaporation, and Gandhidasan [6] studied heat and mass transfer in solar regenerators. The turbulence and the momentum transport in the liquid film were investigated by some researchers [3, 7, 9]. It is noted that a forced convective [1, 3, 6] or a stagnant [2, 4, 7] gas layer in a liquid–gas flow system is generally focused and a linear distribution of temperature (for laminar flow) or a negligible temperature gradient across the liquid film has been suggested by some investigators [6, 8]. The transfer processes both in gas phase and liquid phase are important but numerous researchers only emphasize one of them and neglect the other.

An open-type flat-plate solar collector is a typical gas–liquid system, in which the meteorological quantities, the tilt angle and the liquid film thickness exert an influence on heat, mass and momentum transfer. This

has not been investigated sufficiently. The purpose of this study is to determine the momentum transfer in a falling water film, the heat and mass transfer from the water film to an accompanied gas flow, and to investigate the effects of various parameters including the magnitude of the solar radiation, the atmospheric temperature and humidity, the wind velocity, the absorbing plate tilt angle and the water film thickness on them. A cluster of physical models had been developed, and the characteristics of heat, mass and momentum transfer was revealed through solving the equations numerically.

2. ANALYSIS

The physical model concerned in this study is illustrated in *figure 1*. The water flows down over a tilted plate as a thin film due to the action of gravity. By the actions of viscous and inertial forces, the stagnant ambient atmosphere or the co-current wind will flow along with the water film forming an accompanying gas boundary layer. The solar radiative flux incident upon the free surface of the water film is partly transmitted across the film and it is mainly absorbed by the water film and the absorbing plate which has been coated with black paint ($\alpha^*_{w,\lambda} = 0.94$) and is well insulated from behind. The heat absorbed by the plate then is transferred to the water film and across it partially to the gas layer. When evaporation occurs, mass transfer takes place simultaneously between the water film and the gas layer.

2.1. Governing equations

In general, liquid film flow over a solid surface is a wavy one except in the region near the start of flow or at a very small Reynolds numbers. Besides the statistical approach, nearly all remaining major investigations on the turbulent film flow were based on the constant film thickness model for low rate of evaporation [9], which assumed that film could be treated as smooth so that it could be represented by an average film thickness and that some eddy diffusivity profiles, valid for single-phase flow, could be modified or directly applied to turbulent film flow. The wind velocity in the present study was limited to 5 m·s^{-1}. Therefore for a reference plate length of 1.5 m, the gas-phase Reynolds number, $Re_g = |u_\infty - u_i|\, x/\nu_g$, based on the gas velocity relative to the interfacial velocity is not over the value of $3{\cdot}10^5$ so that the gas stream could be treated as laminar flow. In addition, the damped turbulence zone of the liquid film [9] and the laminar gas stream are matched at the gas-liquid interface. Although some researchers revealed that rippling or the small waves on the base film enhances the mass transfer rate in the gas phase, the results obtained by Hikia et al. showed that the effect of rippling on the gas-phase mass and heat transfer rates is negligible [9]. The inlet water velocity distribution was prescribed at a value for the fully developed flow without interfacial shear.

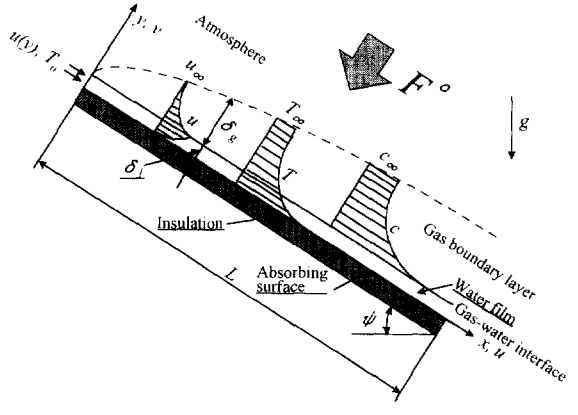

Figure 1. Schematic diagram of the physical system.

In "the constant film thickness model", assuming the boundary concept to be valid and neglecting the pressure gradient, buoyancy force and dissipated heat, the equations for a steady two-dimensional incompressible turbulent flow of the water film are

- mass

$$\frac{\partial u_l}{\partial x} + \frac{\partial v_l}{\partial y} = 0 \tag{1}$$

- momentum

$$u_l \frac{\partial u_l}{\partial x} + v_l \frac{\partial u_l}{\partial y} = \frac{\partial}{\partial y}\left[(\nu_l + \varepsilon_m)\frac{\partial u_l}{\partial y}\right] + g \sin\psi \tag{2}$$

and energy

$$\rho_l c_{p,l} u_l \frac{\partial T_l}{\partial x} + \rho_l c_{p,l} v_l \frac{\partial T_l}{\partial y} = \frac{\partial}{\partial y}\left[\left(k_l + \frac{\rho_l c_{p,l} \varepsilon_m}{Pr_t}\right)\frac{\partial T_l}{\partial y}\right] + \frac{\partial}{\partial y}\left(F^+ - F^-\right) \tag{3}$$

where ε_m, Pr_t, F^+ and F^- are the eddy diffusivity for momentum, the turbulent Prandtl number and the radiative fluxes in the forward (+) and backward (−) directions in the water film, respectively, and these properties will be modeled later. The second term on the right side of equation (3) represents energy transfer due to the film absorption of the solar radiation. The radiative flux gradient acts like a thermal source, which has been neglected in the analysis of Gandhidasan [6].

Neglecting the gas absorption of the solar radiation, then the equations of mass, momentum, energy and concentration in the laminar gas layer can be deduced as

$$\frac{\partial(\rho_g u_g)}{\partial x} + \frac{\partial(\rho_g v_g)}{\partial y} = 0 \tag{4}$$

$$\rho_g u_g \frac{\partial u_g}{\partial x} + \rho_g v_g \frac{\partial u_g}{\partial y} = \frac{\partial}{\partial y}\left(\mu_g \frac{\partial u_g}{\partial y}\right) + g\,(\rho_g - \rho_\infty)\sin\psi \quad (5)$$

$$\rho_g c_{p,g} u_g \frac{\partial T_g}{\partial x} + \rho_g c_{p,g} v_g \frac{\partial T_g}{\partial y} = \frac{\partial}{\partial y}\left(k_g \frac{\partial T_g}{\partial y}\right) + \rho_g D\,(c_{p,v} - c_{p,a}) \frac{\partial c}{\partial y}\frac{\partial T_g}{\partial y} \quad (6)$$

and

$$\rho_g u_g \frac{\partial c}{\partial x} + \rho_g v_g \frac{\partial c}{\partial y} = \frac{\partial}{\partial y}\left(\rho_g D \frac{\partial c}{\partial y}\right) \quad (7)$$

The second term on the right side of equation (6) represents the transport of energy due to the concentration gradient which has not been considered in the analysis of Yan and Soong [1]. Furthermore, it is assumed that the gas mixture exhibits ideal gas law behavior. Neglecting the instantaneous values, the thermal equation of state is written as:

$$p_g = \rho_g T_g R_m \left(\frac{1-c}{M_a} + \frac{c}{M_v}\right) \quad (8)$$

and the specific heat for the binary gas mixture becomes:

$$c_{\mathrm{p,g}} = c_{\mathrm{p,a}} + c\,(c_{\mathrm{p,v}} - c_{\mathrm{p,a}}) \quad (9)$$

where $c_{\mathrm{p,a}}$ and $c_{\mathrm{p,v}}$ denote the specific heats for dry air and water vapor, respectively.

2.2. Boundary and interfacial conditions

The boundary conditions for the problem are

$$x = 0: \quad u_\mathrm{l} = u(y),\ T_\mathrm{l} = T_\mathrm{o},\ u_\mathrm{g} = u_\infty,\ T_\mathrm{g} = T_\infty,\ c = c_\infty \quad (10)$$

$$y = 0: \quad u_\mathrm{l} = 0,\ -\left(k_\mathrm{l} + \frac{\rho_\mathrm{l} c_{\mathrm{p,l}} \varepsilon_\mathrm{m}}{Pr_\mathrm{t}}\right)\frac{\partial T_\mathrm{l}}{\partial y} = \int_0^{\lambda_\mathrm{c}} \alpha^*_{w,\lambda} F^+_\lambda(0)\,\mathrm{d}\lambda \quad (11)$$

and

$$y \to \infty: \quad u_\mathrm{g} = u_\infty,\ T_\mathrm{g} = T_\infty,\ c = c_\infty \quad (12)$$

The term on the right side of equation (11) accounts for the absorption of the external radiation by the opaque plate. The external radiation in the semi-transparent part of the spectrum ($0 \le \lambda < \lambda_\mathrm{c}$) incident on the gas–water interface is partially transmitted across the water film, and it is mainly absorbed by the absorbing plate.

At the gas-water interface ($y = \delta_\mathrm{l}$), the continuities of velocity, temperature and shear stress, and the energy balance must be met, i.e.

$$u_\mathrm{i} = u_\mathrm{l} = u_\mathrm{g} \quad (13)$$

$$T_\mathrm{i} = T_\mathrm{l} = T_\mathrm{g} \quad (14)$$

$$\left[(\mu_\mathrm{l} + \rho_\mathrm{l}\varepsilon_\mathrm{m})\frac{\partial u_\mathrm{l}}{\partial y}\right]_{\mathrm{i,l}} = \left(\mu_\mathrm{g}\frac{\partial u_\mathrm{g}}{\partial y}\right)_{\mathrm{i,g}} \quad (15)$$

and

$$\int_{\lambda_\mathrm{c}}^{\infty} \alpha^*_{\mathrm{i},\lambda} F^\mathrm{o}_\lambda\,\mathrm{d}\lambda - \left[\left(k_\mathrm{l} + \frac{\rho_\mathrm{l} c_{\mathrm{p,l}} \varepsilon_\mathrm{m}}{Pr_\mathrm{t}}\right)\frac{\partial T_\mathrm{l}}{\partial y}\right]_{\mathrm{i,l}} = h_{\mathrm{fg}}\, m - \left(k_\mathrm{g}\frac{\partial T_\mathrm{g}}{\partial y}\right)_{\mathrm{i,g}} \quad (16)$$

By considering the solubility of air in the water film to be negligibly small, the transverse velocity of the air–vapor mixture in the gas–water interface can be expressed as

$$v_\mathrm{i} = -\left(\frac{D}{1-c}\frac{\partial c}{\partial y}\right)_{\mathrm{i,g}} \quad (17)$$

and the mass flux from the water film to the gas layer,

$$m = \rho_{\mathrm{i,g}}\, v_\mathrm{i} \quad (18)$$

Assuming the gas–water interface at saturation pressure, $p_{\mathrm{i,v}}$, the interfacial mass fraction of water vapor can be evaluated by [10]

$$c_\mathrm{i} = \frac{p_{\mathrm{i,v}}}{(p - p_{\mathrm{i,v}})\dfrac{M_\mathrm{a}}{M_\mathrm{v}} + p_{\mathrm{i,v}}} \quad (19)$$

where M_a and M_v denote the molar mass of dry air and vapor, respectively. The partial pressure of the saturation water vapor at the gas-water interface is estimated from Antoine's correlation [11]

$$p_{\mathrm{i,v}} = 133.32 \exp\left(18.3036 - \frac{3\,816.44}{T_\mathrm{i} - 46.13}\right) \quad (20)$$

2.3. Radiative transfer model

Both gas and water are semi-transparent to radiation. They are transparent in the visible and infrared part of the spectrum, and scattering is negligible in comparison to absorption. To simplify the model, it is assumed in the analysis that the gas-water and the water-plate interfaces are smooth and the absorption of solar radiation in the gas layer is negligibly small, which is based on the fact that the mass fraction of water vapor in this study does not exceed 0.0156 and the total absorptivity of the gas layer is less than 0.001 [12]. If emission of radiation by the water is neglected in comparison to absorption, and the forward scattering approximation (i.e., radiation is scattered in the forward direction only) is used, the forward (+) and backward

(−) directed radiative fluxes in the water film (*figure 2*) can be expressed as [13]

$$F^{+} = \int_0^{\lambda_c} F_\lambda^{+}(y)\,\mathrm{d}\lambda = \int_0^{\lambda_c} \tau_\lambda^{*}\, F_\lambda^{o}\, \mathrm{e}^{-\beta_\lambda(\delta_l - y)}\, \gamma_\lambda\,\mathrm{d}\lambda \tag{21}$$

and

$$F^{-} = \int_0^{\lambda_c} F_\lambda^{-}(y)\,\mathrm{d}\lambda = \int_0^{\lambda_c} \rho_{w,\lambda}^{*}\, \tau_\lambda^{*}\, F_\lambda^{o}\, \mathrm{e}^{-\beta_\lambda(\delta_l + y)}\, \gamma_\lambda\,\mathrm{d}\lambda \tag{22}$$

respectively. In these equations

$$\gamma_\lambda = [1 - \rho_{w,\lambda}^{*}\,\rho_{i,\lambda}^{*}\exp(-2\beta_\lambda\,\delta_l)]^{-1} \tag{23}$$

is a parameter which accounts for inter-reflection of radiation between the gas-water interface and the absorbing plate surface.

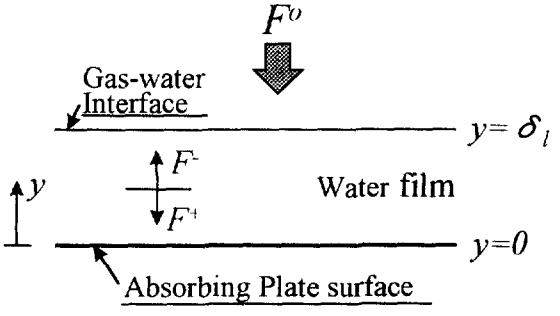

Figure 2. Schematic of the radiation model.

2.4. Turbulence model

A lot of turbulence models for determining the eddy diffusivity for the momentum of a falling film have been developed by many investigators [14–18]. In view of the theory of eddy diffusivity damping near the gas-liquid interface[9, 19–21], the modified van Driest model suggested by Yih and Liu [14] and the interface damping eddy diffusivity model deduced by Bin [19] are adopted herein. Therefore the eddy diffusivity for momentum is divided into three regions, for $y/\delta_l \le 0.6$,

$$\frac{\varepsilon_m}{\nu_l} = -0.5 + 0.5\left\{1 + 0.64\,y^{+2}\frac{\tau}{\tau_w}\left[1 - \exp\left(-\frac{y^+}{A^+}\left(\frac{\tau}{\tau_w}\right)^{\frac{1}{2}}\right)\right]^2 f^2\right\}^{\frac{1}{2}} \tag{24}$$

where $f = \exp(-1.66y^{+}/\delta_l^{+})$ is a damping factor. For $0.6 < y/\delta_l \le y_c/\delta_l$, the eddy diffusivity is taken as constant and equal to its value at $y/\delta_l = 0.6$,

$$\frac{\varepsilon_m}{\nu_l} = \left.\frac{\varepsilon_m}{\nu_l}\right|_{y/\delta_l = 0.6} \tag{25}$$

and for $y/\delta_l > y_c/\delta_l$,

$$\frac{\varepsilon_m}{\nu_l} = 1.17\cdot 10^{-6}\left(\frac{g}{\nu_l^2}\right)^{\frac{2}{3}} Re^{1.448}(\delta_l - y)^2 \tag{26}$$

where y_c is the intersecting point at which the two eddy diffusivity models reach a same value. The effect of the interfacial shear stress is considered in the model. It is noted that the directions of the interfacial shear stress under the condition of stagnant atmosphere are just opposite to those in the model analyzed by Yih and Liu [14].

There are some formulae provided by some investigators for estimating the turbulent Prandtl number [14, 18, 22, 23]. In order to correspond to the eddy diffusivity model adopted, the van Driest style turbulent Prandtl number modified by Yih and Liu [14] is used in this work. The turbulent Prandtl number is evaluated by

$$Pr_t = \frac{1 - \exp[-y^{+}(\tau/\tau_w)^{\frac{1}{2}}/A^{+}]}{1 - \exp[-y^{+}(\tau/\tau_w)^{\frac{1}{2}}/B^{+}]} \tag{27}$$

where B^{+} is given by Habib and Na [14] as

$$B^{+} = Pr^{-\frac{1}{2}}\sum_{n=1}^{5} b_n\,(\log Pr)^{n-1} \tag{28}$$

where $b_1 = 34.96$, $b_2 = 28.97$, $b_3 = 33.95$, $b_4 = 6.33$, and $b_5 = -1.186$.

2.5. Thermodynamic, transport and radiation properties

The variations of thermodynamic and transport properties with temperature and mixture composition in the present study are considered except that the water density is treated as constant. The transport properties for air [24] are used as follows:

$$\mu_a = \frac{14.58\cdot 10^{-7}\,T^{\frac{3}{2}}}{110.4 + T} \tag{29}$$

$$k_a = \frac{2.6482\cdot 10^{-3}\,T^{\frac{3}{2}}}{T + 245.4\times 10^{-\frac{12}{T}}} \tag{30}$$

and

$$c_{p,a} = 917 + 0.258\,T - 3.98\cdot 10^{-5}\,T^2 \tag{31}$$

Other pure component data including the latent heat of vaporization of water are approximated by polynomials in terms of temperature and the mixture properties are calculated from the pure component data by means of the mixing rule, taken from Reid et al. [11].

Water is a selective absorber of radiation and its volumetric radiation property was taken from Brewster

[12]. The cutoff wavelength for water is assumed to be $\lambda_c = 2.5$ μm. The radiation surface properties of water and the plate were taken from available literature sources [10, 12].

3. SOLUTION METHOD

A control-volume finite-difference procedure [25] was used to solve the coupling equations. A fully implicit numerical scheme was employed. In order to obtain an accurate solution, the convective term is approximated by a power-law form. Moreover, in view of the study performed by Yan and Soong [1], a grid of 152 × 602 points was used across the water film and gas layer thickness for water film thickness of $1{\cdot}10^{-3}$ m and 152 × 1 202 grid for $\delta_l = 5{\cdot}10^{-4}$ m. Of the 602 or 1202 axial grid lines, 51 were deployed on the water side. The grids used in gas and water phases are identical and uniform except for those next to the inlet, the plate surface and the gas-water interface, which were packed with only half the normal space. Solutions were found to be insensitive for the grid number over 100×40 across the water film.

The system of algebraic discretization equations obtained for water and gas regions was solved through the line-by-line application of the tri-diagonal matrix algorithm. It is noted that at the gas-water interface the matching discretization equations were set up by making momentum and energy balances. To avoid the divergence of iterations, the time interval in the discretization equations for unsteady problems was chosen as a specific under-relaxation factor together with another normal under-relaxation factor to solve the present steady problem, which were changed from 0.003 and 0.86 to 0.009 and 0.46 during the calculation process.

The total radiation fluxes were evaluated numerically using a spectral-band model. A total of only 21 spectral bands was used because a more detailed spectral distribution of incident radiation flux was not available [26].

4. RESULTS AND DISCUSSION

The system parameters or the boundary conditions are important to the system analysis. Considering the climate condition which changes with season, geographic position, solar time and etc. [27, 28], we chose the parameters ranges in this study as: $30° \le \psi \le 60°$, $0 \le F° \le 1\,190$ W·m^{-2}, $5{\cdot}10^{-4} \le \delta_l \le 1.5{\cdot}10^{-3}$ m, $288 \le T_\infty \le 298$ K, $0.003 \le c_\infty \le 0.014$, $0 \le u_\infty \le 5$ m·s^{-1} and $T_0 = 293.15$ K. The plate reference length L was selected as 1.5 m.

Figure 3 shows the typical transverse (y-direction) distributions of the water flow velocity, u_l, and temperature, T_l, at $X = 0.6567$ for a stagnant atmosphere ($u_\infty = 0$ m·s^{-1}). The data reveal the common characteristics of the velocity and temperature profiles for turbulent water film flow. The heat loss from the free surface of the water film causes an obvious drop in temperature near the interface.

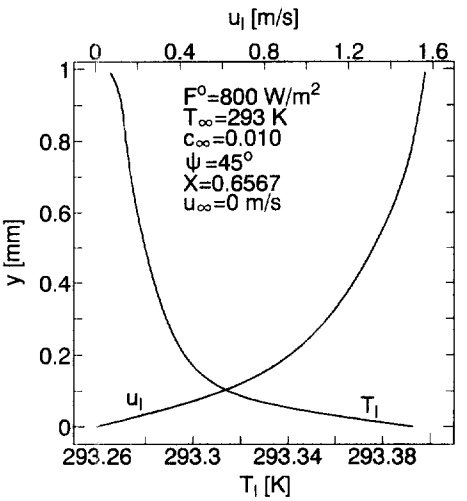

Figure 3. Typical transverse distributions of water flow velocity and temperature.

The typical transverse distributions of ε_m/ν_l and Pr_t for different film thickness, δ_l, are plotted in *figures 4a* and *4b*. The eddy diffusivity for momentum reaches its maximum at about 0.45 of the film thickness. The values of eddy diffusivity and the intersecting point of the two eddy diffusivity models increase with increasing film thickness. The water film Reynolds numbers, Re, are 1011, 4653, and 9739 corresponding to a water film thickness of $5{\cdot}10^{-4}$ m, $1{\cdot}10^{-3}$ m, and $1.5{\cdot}10^{-3}$ m, respectively. In contrast, the turbulent Prandtl number decreases with an increase in the Reynolds number, and reaches its minimum at the position around 0.75 δ_l. For $Re = 1\,011$, the eddy diffusivity for momentum is less than one third of the kinematic viscosity. The effects of different angles on the eddy diffusivity and the turbulent Prandtl number are similar to those of different film thickness.

Figure 5 presents the axial distributions of average water velocity for different wind velocities. Near the entrance region, the average water velocity, u_{av}, first rises or drops dramatically from an initial value of 1.1875 m·s^{-1} to its maximum or minimum according to whether the wind velocity is greater or smaller than the gas-water interfacial velocity, then drops or rises at variable rates. If the wind velocity is just moderately larger than the interfacial velocity, the average velocity after reaching its maximum may drop

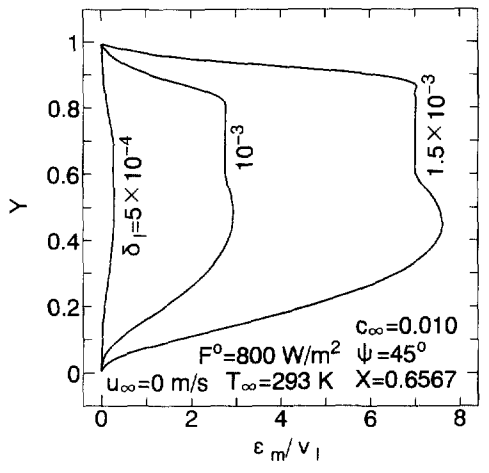

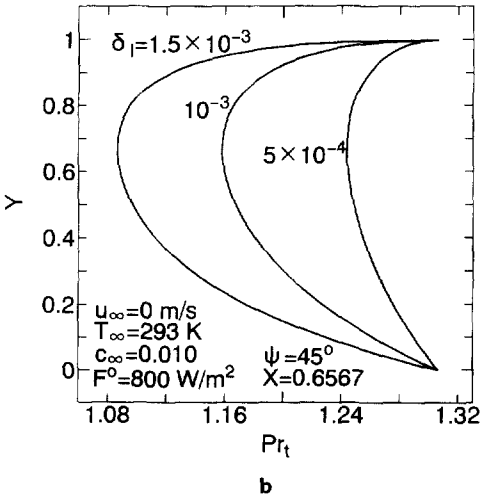

Figure 4. a. Typical transverse distributions of ε_m/ν_l for different δ_l. **b.** Typical transverse distributions of Pr_t for different δ_l.

to a minimum at a certain position (see the data in *figure 5* for $u_\infty = 2$ m·s^{-1}). The velocity development tendencies for the same direction of the interfacial shear stress e.g. with the condition of $u_\infty = 0$ and $u_\infty = 1$ m·s^{-1} or $u_\infty = 2$ m·s^{-1} and $u_\infty = 5$ m·s^{-1} are similar to each other. As the wind velocity is greater than the interfacial velocity, the stronger plate surface shear stress ($\tau_w = \rho_l g \delta_l \sin\psi + \tau_i$) and water shear stress (at the position of y, $\tau = \rho_l g (\delta_l - y) \sin\psi + \tau_i$) will stagnate the water film flow after it reaches its maximum by the action of interfacial shear stress. On the other hand, if the wind velocity is smaller than the interfacial velocity, the weaker plate surface shear stress ($\tau_w = \rho_l g \delta_l \sin\psi - \tau_i$) and the water shear stress (at the position of y, $\tau = \rho_l g (\delta_l - y) \sin\psi - \tau_i$) cannot balance the gravitational and inertial forces so that the water film flow after touching its bottom will be accelerated.

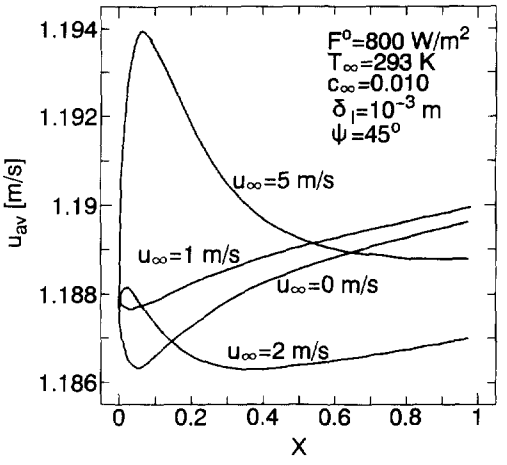

Figure 5. Typical axial distributions of u_{av} for different u_∞.

The temperature and turbulence of the water film also make some contributions to the variation in the average water velocity due to the effective viscosity. The obtained results reveal an interesting phenomenon that the higher wind velocity can get a lower average water velocity than its initial value except for the entrance region, and the lower wind velocity might reach a higher value of the average water velocity in the region developed later. It should be noted that the change in average water velocity in the flow direction does not exceed 0.55 % of its initial value.

Typical transverse distributions of velocity and concentration at two X positions for stagnant atmosphere condition are shown in *figure 6*. Although the variation of the average water velocity along the flow direction is presented in *figure 5*, the velocity profiles in the water film at $X = 0.0433$ and $X = 0.6567$ overlap each other. This can be attributed to the fact that the scale of the velocity coordinate used in *figure 6* is much larger than that used *figure 5* so that the small relative difference (less than 0.5 %) in water velocity for different X can not be identified in *figure 6*. The profiles of velocity and concentration in the gas boundary layer are similar at the same X position but they differ to a great extent from each other for different X positions. In the early developing region of the gas boundary layer ($X = 0.0433$), both velocity and the mass fraction of water vapor vary sharply towards the atmospheric parameters, while the changes in velocity and water vapor mass fraction in the developed gas boundary layer region ($X = 0.6567$) are rather moderate.

Figure 7 provides the profiles of temperature and the mass fraction of water vapor at two different X positions, respectively. Though the velocity profiles across the water film thickness are almost the same for different X positions as shown in *figure 6*, the temperature profiles in the water film at different X positions are different from each other. As X increases, the continuous solar heating brings about a rise in

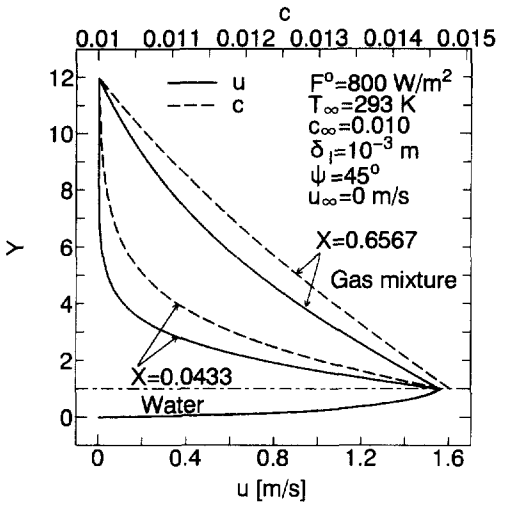

Figure 6. Typical transverse distributions of u and c at two X positions.

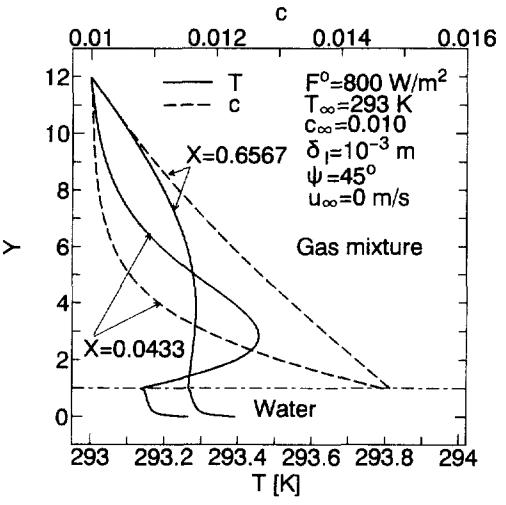

Figure 7. Typical transverse distributions of T and c at two X positions.

the water temperature. At the early developing region of the gas boundary layer ($X = 0.0433$), the high evaporation rate of water causes an obvious drop of water temperature near the gas-water interface. The energy transport in the gas mixture is done by means of conduction, convection and diffusion. Under the conditions of moderate ambient humidity ($RH = 70$ %) and around the same value of the atmospheric temperature as the entrance temperature of the water film ($T_\infty = 293$ K, $T_0 = 293.15$ K), the temperature profile in the gas layer reaches a maximum at certain positions ($Y = 3$ for $X = 0.0433$; $Y = 4$ for $X = 0.6567$). This can be explained by the fact that the water vapor carrying a lot of heat from the gas-water interface, releases heat whilst decreasing its mass fraction on the way outside, which causes the gas temperature to reach a maximum. The specific heat and density of gas is quite small as compared with those of water so that the maximum gas temperature could be higher than the plate surface temperature.

The effects of atmospheric humidity and temperature on the transverse distributions of temperature and the mass fraction of water vapor in the gas layer at two X positions are presented in *figures 8a* and *8b*, respectively. It is understood from *figure 8a* that the variation of temperature is similar to that of the mass fraction of water vapor at the same X direction. Under the condition of high atmospheric humidity ($c_\infty = 0.014$, $RH = 96$ %), which means a small vapor concentration gradient $\partial c/\partial y$, the energy transport in the gas layer is so small that it is not enough to reach a maximum temperature (see *figure 8a*). As the atmospheric temperature of 288 K is about 5 K lower than the water entrance temperature, the energy transferred by the concentration gradient is overshadowed in the larger temperature gradient and also can not raise a temperature maximum (see *figure 8b*).

The wind velocity dramatically influences the distribution of the mass fraction of water vapor in the gas boundary layer. The data plotted in *figure 9* show that the profile of water vapor mass fraction at the same X position for $u_\infty = 5$ m·s^{-1} has a flatter shape than that for $u_\infty = 0$ m·s^{-1}. It is obvious that the higher intensity of the forced convection makes the gas boundary layer thinner which further enhances the mass transfer.

Figures 10a to *10f* show the variations of the absorbing plate surface temperature, T_w, and the gas-water interfacial temperature, T_i, with dimensionless coordinate, X, under the various conditions of the solar incident flux, F°, the mass fraction of water vapor in the ambient atmosphere, c_∞, the atmospheric temperature, T_∞, the tilt angle, ψ, the water film thickness, δ_l, and the wind velocity, u_∞, respectively. As expected, continuous radiant heating raises both T_w and T_i along the flow direction except in the neighborhood of $X = 0$, in which the high evaporation rate brings about a drop in the interfacial temperature to keep energy balance. The magnitude of the drop in T_i mainly depends on the ambient temperature, humidity and wind velocity. Either a decrease in c_∞ or T_∞, or an increase in u_∞ will lead to an increase in the magnitude of the drop in T_i, which has been shown in *figures 10b, 10c,* and *10f*. This can be attributed to the decrease in c_∞ or T_∞, or the increase in u_∞ which obviously enhances the heat and mass transmission from the gas-water interface to the gas boundary layer. For $F^\circ = 0$, both T_i and T_w have no way of rising but dropping down along the flow direction as the water evaporation absorbs the energy from the water film. At the position near the inlet ($X = 0$), the plate surface temperature, T_w, rises dramatically to a certain value, which depends on the magnitude of solar incident flux (*figure 10a*), the thickness of water

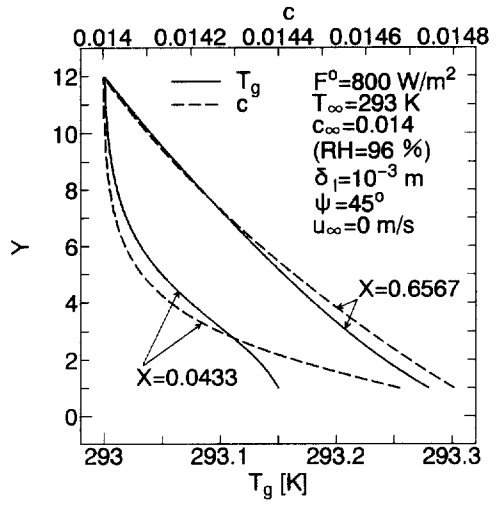

Figure 8. a. Effects of high atmospheric humidity on the distributions of T_g and c at two X positions. **b.** Effects of lower atmospheric temperature on the distributions of T_g and c at two X positions.

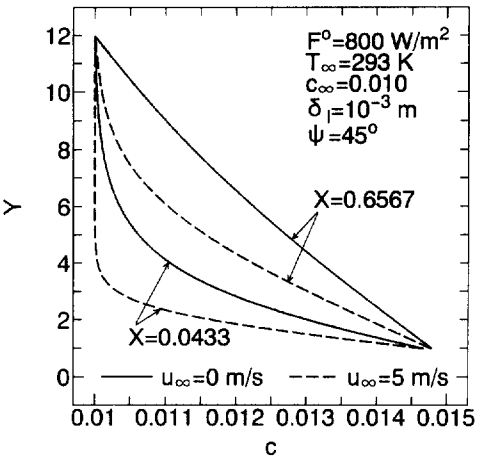

Figure 9. Effects of u_∞ on the distributions of c at two X positions.

film (*figure 10e*) and the plate tilt angle (*figure 10d*), and then rises along the flow direction at a lower rate according to the ambient conditions. In the latter developed region of the boundary layer, the variations of T_w and T_i with X are almost linear. These results indicate that the magnitude of heat and mass transfer remain nearly constant in the developed region. An increase in the solar incident flux, F°, the mass fraction of water vapor in ambient atmosphere, c_∞, the atmospheric temperature, T_∞, and/or a decrease in wind velocity, u_∞, will result in the rise of the gas-water interface temperature, T_i, and the plate surface temperature, T_w. The tilt angle, ψ, represents the influence of the gravitational force. The gravitational force with an increase in ψ plays a more important role in the hydrodynamic force, which increases the flow rate of the water film so that the time spent by wafer flowing across the plate length is shortened, and the magnitude of the temperature rise of the water film will be limited. The effects of δ_l on T_i and T_w are analysed in two ways; one is changing the thermal capacity of the water film, and the other the flow rate. Therefore an increase in δ_l would reduce the rise in T_i and T_w along with X as seen in *figure 10e*.

The variations of interfacial mass fraction of water vapor, c_i, with dimensionless coordinate, X, for some tilt angles, ψ, are plotted in *figure 11*. Comparing these with the data in *figure 10d*, it is clear that the tendency of the axial distribution of c_i is quite similar to that of T_i, in view of the relation of $c_i = f(T_i)$.

The mass and heat fluxes at the gas-water interface are the most dominant parameters for mass and heat transfer from the water film to the gas layer. The total interfacial heat flux, q_x, consists of two parts; one is sensible heat flux, q_s, and the other is latent heat flux, q_l. It can be expressed as

$$q_x = q_l + q_s = h_{fg} m - \left(k_g \frac{\partial T_g}{\partial y} \right)_{i,g} \qquad (32)$$

The variations of interfacial mass flux, m, with X for various parameters c_∞, δ_l, and u_∞ are shown in *figures 12a* to *12c*. The interfacial mass flux decreases sharply in the range of $X < 0.2$, and beyond $X = 0.2$, it reaches a certain value according to c_∞, δ_l, and u_∞. The value of m and its variation for each parameter would be mainly dependent on the concentration gradient in the gas boundary layer and the wind velocity. The lower atmospheric humidity ($c_\infty = 0.003$, $RH = 20$ %) causes

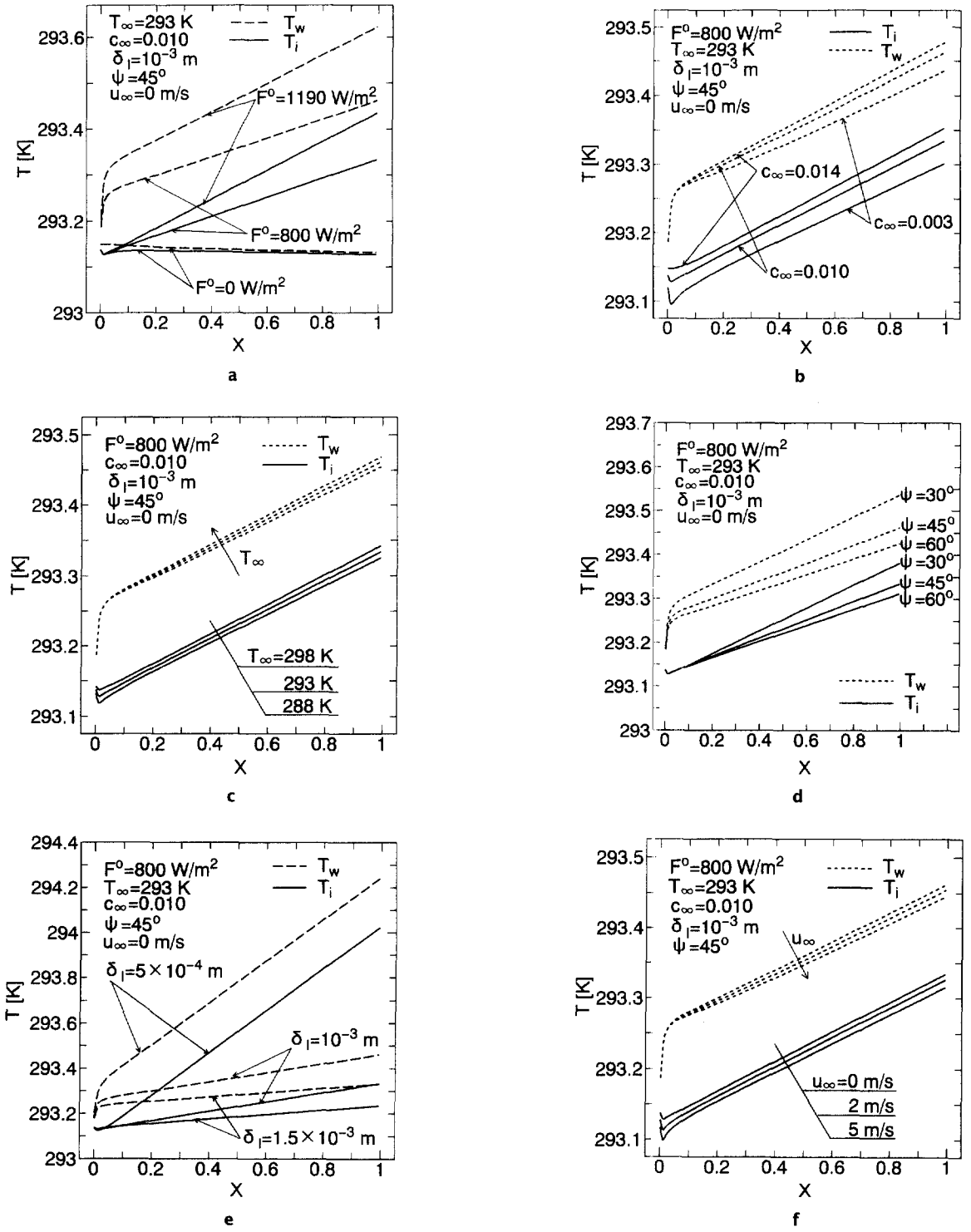

Figure 10. **a.** Effects of F° on T_w and T_i. **b.** Effects of c_∞ on T_w and T_i. **c.** Effects of T_∞ on T_w and T_i. **d.** Effects of ψ on T_w and T_i. **e.** Effects of δ_l on T_w and T_i. **f.** Effects of u_∞ on T_w and T_i.

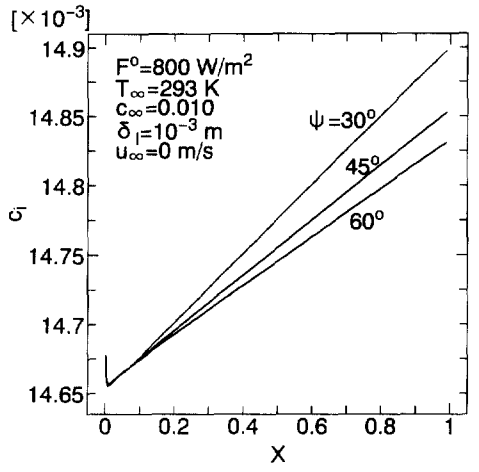

Figure 11. Effect of ψ on c_i.

a higher concentration gradient in the gas boundary layer so that the value of m at the outlet of the water flow is still higher than 0.0416 g·m^{-2}·s^{-1}. However under the condition of $c_\infty = 0.014$ ($RH = 96\%$), m is only 0.00365 g·m^{-2}·s^{-1} at the outlet (*figure 12a*). The increase in δ_l, or u_∞ raises the gas flow velocity so that the mass transfer is enhanced and m can arrive at a higher value (see *figure 12b* and *12c*). It is noted that the change in the wind velocity directly affects the gas velocity so that its effect on mass flux is more obvious than those of the water film thickness and the plate tilt angle. The effects of F° and T_∞ on m are only dependent on the variation in the interfacial mass fraction of water vapor along the flow direction, which is not intensive in the open-type collector. Therefore their influences on m are negligibly small.

Based on the data in *figures 5*, and *12*, it is concluded that the change in the water film thickness along the plate due to the variation of the water flow velocity and the film evaporation is not more than 0.6 %. Therefore the constant film thickness model used in this study is reasonable.

Figure 13 show the variations of dimensionless heat flux q_s/F°, q_l/F°, and q_x/F° with X for various values of c_∞, T_∞, u_∞. The tendency of the variation of q_l/F° or q_x/F° with X in *figure 13a* is associated with that of m in *figure 12a*. This can be explained by the fact that q_l or q_x is a function of m. *figure 13a* reveals that the ambient humidity exerts an influence on interfacial heat flux, q_x or q_l. When the mass fraction of water vapor in the ambient atmosphere, c_∞, is 0.014 ($RH = 96$ %), the heat loss rate, q_x/F°, from the water film is only about 1.3 % of the incident radiative flux in the region of $X > 0.2$. However as c_∞ reduces to 0.003 ($RH = 20$ %),

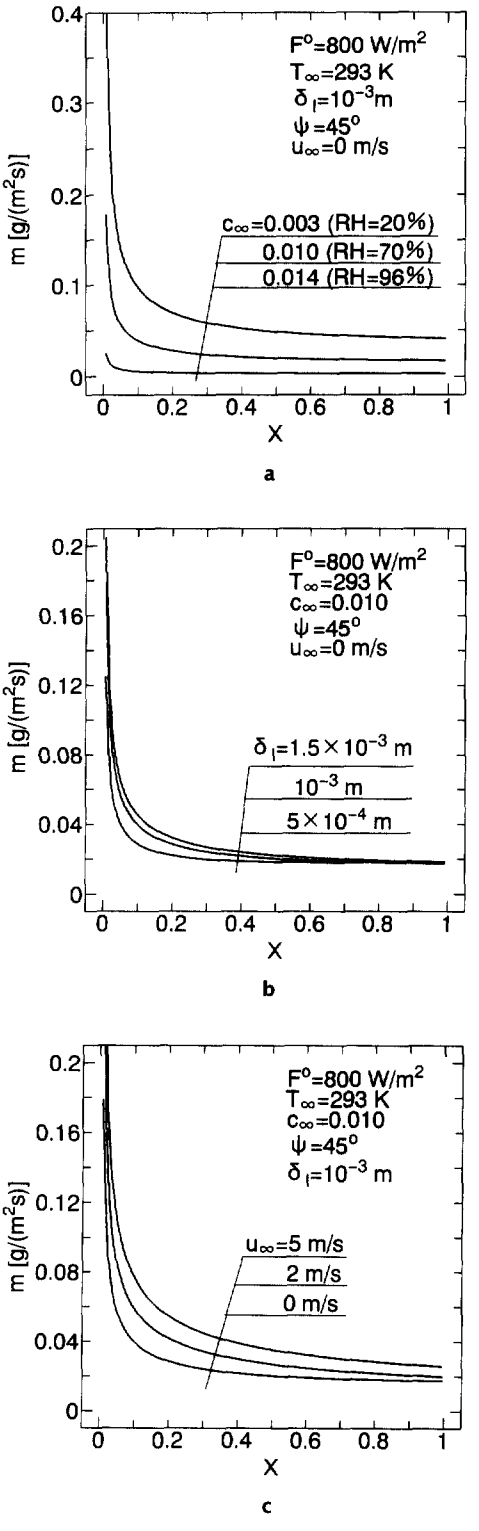

Figure 12. a. Effect of c_∞ on m. **b.** Effect of δ_l on m. **c.** Effect of u_∞ on m.

q_x/F^o reaches a very high value of around 12.7 % even at the outlet of the water flow. The data also show that the latent heat flux could be higher than the total heat flux in a wider region for a lower atmospheric humidity. From the results of *figure 13b*, it is noticed that the ambient temperature, T_∞, dramatically affects the heat loss rate, q_s/F^o, but its influence on q_l/F^o is negligibly small. Under the condition of $T_\infty \approx T_0$, q_s/F^o is very small, which keeps negative in the region of $X < 0.7$ and reaches a value only around 0.08 % at the outlet. However as T_∞ of 288 K is about 5 K less than T_0, q_s/F^o can reach a value of around 1.78 % at the outlet. On the other hand, if T_∞ of 298 K is about 5 K higher than T_0, the value of q_s/F^o approaches about -1.68 % at the outlet, which means that the sensible heat is transferred from the gas layer to the water film. Even though around a 5 K difference in entrance water and ambient atmosphere temperatures provides a higher value of sensible heat flux, it is still less than one third of the value of latent heat flux in most of the flow region. The effect of wind velocity on the heat loss of the water film is so intensive that the total heat fluxes from the water film to the gas layer at $X = 0.5$ for $u_\infty = 5$ m·s^{-1} and $u_\infty = 2$ m·s^{-1} could be 1.73 and 1.32 times as high as that for stagnant atmosphere ($u_\infty = 0$ m·s^{-1}), respectively (see *figure 13c*).

The rate of heat and mass transfer can be also expressed with the heat and mass transfer coefficients or Nusselt and Sherwood numbers as non-dimensional parameter. We defined the interfacial heat transfer coefficients as corresponding to sensible, h_s, latent, h_l, and overall, h_x, heat transfers, respectively, as follows:

$$h_s = \left| \frac{q_s}{T_i - T_\infty} \right| \tag{33}$$

$$h_l = \frac{q_l}{|T_i - T_\infty|} \tag{34}$$

$$h_x = \frac{q_x}{|T_i - T_\infty|} \tag{35}$$

The interfacial mass transfer coefficient, h_m, is defined as

$$h_m = \frac{m}{|\rho_{i,g}\, c_i - \rho_\infty\, c_\infty|} \tag{36}$$

Figure 14 presents the variations of h_s and h_l with X for different atmospheric temperatures, T_∞. The data reveal that h_l is about 3 times greater than h_s. In the region of $0 \le X \le 0.2$, both h_l and h_s drop rapidly, and over $X = 0.2$, their decreasing rates become smooth. From *figure 13b*, it is noted that the atmospheric temperature almost does not influence the latent heat flux. However its effects on interfacial temperature causes the values of h_l for $T_\infty = 298$ K and for $T_\infty = 288$ K to separate from each other along the flow direction. On the one hand,

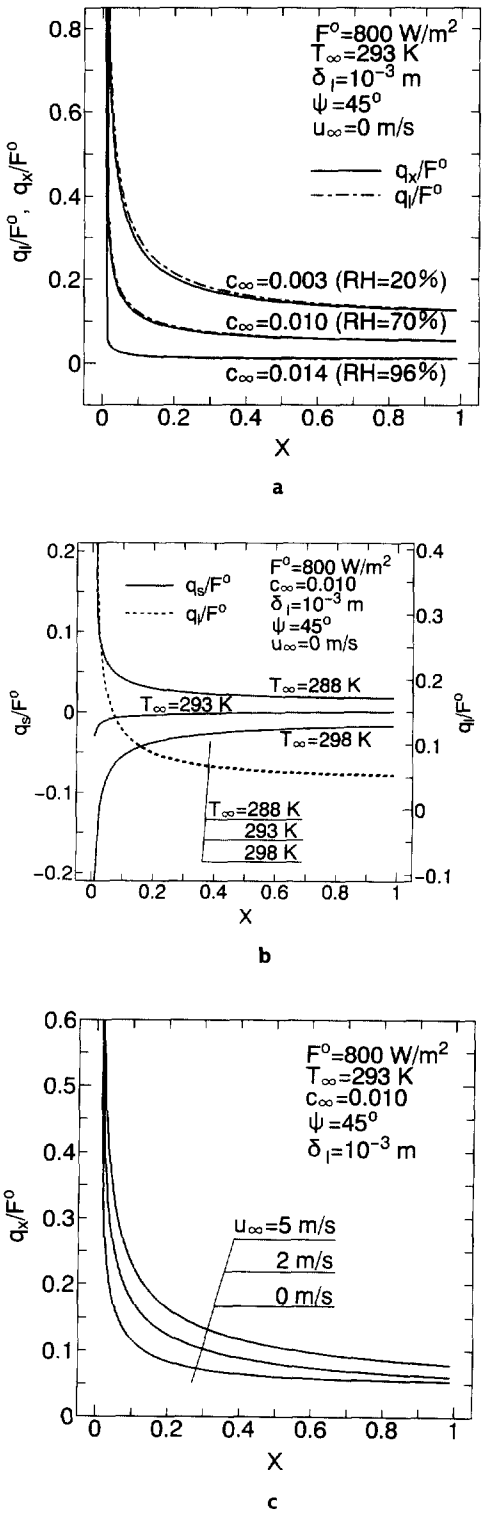

Figure 13. a. Effects of c_∞ on q_l/F^o and q_x/F^o. **b.** Effects of T_∞ on q_s/F^o and q_l/F^o. **c.** Effect of u_∞ on q_x/F^o.

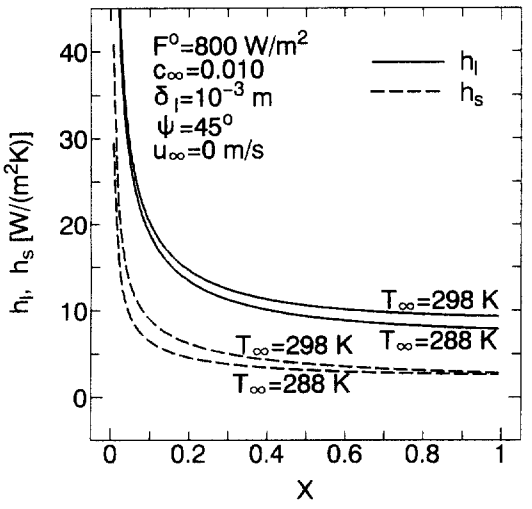

Figure 14. Effects of T_∞ on h_s and h_l.

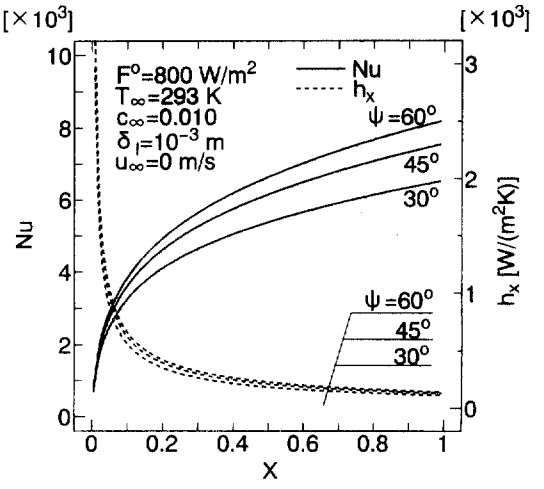

Figure 15. Effects of ψ on h_x and Nu.

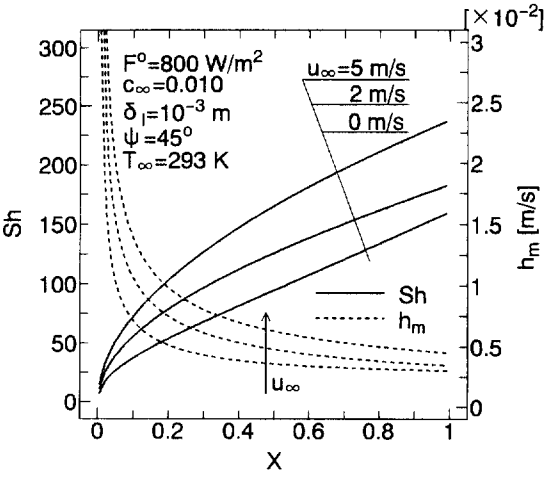

Figure 16. Effects of u_∞ on h_m and Sh.

the partial action of the heat transported due to the concentration gradient on sensible heat transfer makes the gas heating more powerful, and on the other hand, the increase in interfacial temperature along the flow direction enhances the sensible heat transfer in the process of releasing heat but stagnates the sensible heat transfer in the process of gaining heat. Therefore the difference of h_s for $T_\infty = 298$ K and $T_\infty = 288$ K at the entrance region is greater and gradually reduces with an increase in X.

The variations of Nu and h_x with X for different tilt angle, ψ, are shown in *figures 15*. From the data, it should be noted that the Nusselt number and the heat transfer coefficient increase with an increase in the tilt angle, ψ. This could be explained by the fact that an increase in ψ results in an increase in flow velocity which enhances the heat transfer. The interfacial heat and mass fluxes present the same developing tendency as the heat transfer coefficient. From the data shown in *figure 15* and above analysis, it can be concluded that the effects of the plate tilt angle on heat and mass transfer is insignificant.

The data of Sh versus X for different wind velocities, u_∞, are plotted in *figure 16*. From the result of *figure 16*, it is found that an increase in u_∞ enhances the mass transfer. The investigation also indicates that the effects of the solar incident flux on the mass transfer coefficient and Sherwood number are negligibly small.

5. CONCLUSIONS

The heat, mass and momentum transfers of a water film flowing down a tilted plate with solar radiant heating and water evaporation have been studied numerically in this paper. The effects of various parameters on them were investigated. From the results and discussion, the following conclusions can be drawn.

It was clear from numerical results that among the influential factors of heat and mass transfer, the gradients of water vapor mass fraction and temperature between the gas-water interface and the ambient atmosphere as well as the wind velocity played an important role. The water evaporation dominated the process of heat and mass transfer from the water film to the gas layer so that the latent heat flux could be even a little higher than the total heat flux, for the condition that the atmospheric temperature was about the same as the inlet water film temperature. This meant that an maximum temperature might be formed from the heat transportation due to the concentration gradient at a certain position of the gas boundary layer, and the latent heat flux would be partially changed to the

negative sensible heat flux. Although the atmospheric temperature exerted little influence on the interfacial mass flux and the interfacial latent heat flux, it had an obvious effect on the interfacial sensible heat flux.

The magnitude of solar radiative flux incident on the gas-water interface played an important role in changing water temperature but exerted an insignificant influence on interfacial heat and mass transfer.

The water film thickness and the plate tilt angle dramatically influenced the momentum transfer in the water film – the eddy diffusivity for momentum and the turbulent Prandtl number. However their influences on heat and mass transfer were not intensive even if they markedly affected the change in water temperature in the flow direction by means of changing the flow velocity and heat capacity.

Acknowledgements

The financial support of this work by the Patedison Co. Ldt, with T. Takahashi serving as the president, is greatly acknowledged. The first author was a visiting scholar from the People's Republic of China. He is grateful to the China Flight Test Establishment (Xi'an, China) for supporting him during the course of this study.

REFERENCES

[1] Yan W.M., Soong C.Y., Convective heat and mass transfer along an inclined heated plate with film evaporation, Int. J. Heat Mass Tran. 38 (1995) 1261–1269.

[2] Karapantios T.D., Kostoglou M., Karabelas A.J., Local condensation rates of steam–air mixtures in direct contact with a falling liquid film, Int. J. Heat Mass Tran. 38 (1995) 779–794.

[3] Schröppel J., Thiele F., Unterlöhner O., Mass, heat, and momentum transfer in laminar and turbulent pipe flow with vaporization of a liquid film, in: Lewis R.W., Morgan K., Schrefler B.A. (Eds.), Numerical Methods in Thermal Problems, Vol. II, Pineridge Press, Swansea, 1981, pp. 1215–1226.

[4] Faghri A., Prediction of heat and mass transfer for absorption of a gas to a liquid film, in: Lewis R.W., Johnson J.A., Smith W.R. (Eds.), Numerical Methods in Thermal Problems, Vol. III, Pineridge Press, Swansea, 1983, pp. 980–990.

[5] Yang R., Jou D., Heat and mass transfer of absorption process for the falling film flow inside a porous medium, Int. J. Heat Mass Tran. 38 (1995) 1121–1126.

[6] Gandhidasan P., Heat and mass transfer in solar regenerators, in: Cheremisinoff N.P. (Ed.), Handbook of Heat and Mass Transfer, Vol. 2, Gulf Publishing Company, Houston, 1986, Chapter 37.

[7] Grossman G., Heat and mass transfer in film absorption, in: Cheremisinoff N.P., Handbook of Heat and Mass Transfer, Vol. 2, Gulf Publishing Company, Houston, 1986, Chapter 6.

[8] Fujita Y., Tsutui M., Evaporation heat transfer of falling films on horizontal tube (1st report), Trans. JSME (B) 60 (1994) 3469–3474 (in Japanese).

[9] Yih S.M., Modeling heat and mass transport in falling liquid films, in: Cheremisinoff N.P. (Ed.), Handbook of Heat and Mass Transfer, Vol. 2, Gulf Publishing Company, Houston, 1986, Chapter 5.

[10] Eckert E.R.G., Drake R.M. Jr., Analysis of Heat and Mass Transfer, McGraw-Hill, Kogakusha, Tokyo, 1972.

[11] Reid R.C., Prausnitz J.M., Sherwood T.K., The Properties of Gases and Liquids, 3rd edition, McGraw-Hill, New York, 1977.

[12] Brewster M.Q., Thermal Radiative Transfer and Properties, John Wiley & Sons, New York, 1992.

[13] Song B., Viskanta R., Deicing of solids using radiant heating, AIAA J. Thermophys. 4 (1990) 311–317.

[14] Yih S.M., Liu J.L., Prediction of heat transfer in turbulent falling liquid films with or without interfacial shear, AIChE J. 29 (1983) 903–909.

[15] Schlichting H., Boundary-layer Theory (translated by J. Kestin), 7th edition, McGraw-Hill, New York, 1979.

[16] Anderson D.A., Tannehill J.C., Pletcher R., Computational Fluid Mechanics and Heat Transfer, Hemisphere/McGraw-Hill, New York, 1984.

[17] Kumada T., Principles of heat and mass transfer with liquid evaporation, in: Cheremisinoff N.P. (Ed.), Handbook of Heat and Mass Transfer, Vol. 1, Gulf Publishing Company, Houston, 1986, Chapter 7.

[18] Lee S.L., Liquid metal heat transfer in turbulent pipe flows, in: Cheremisinoff N.P. (Ed.), Handbook of Heat and Mass Transfer, Vol. 1, Gulf Publishing Company, Houston, 1986, Chapter 12.

[19] Bin A.K., Mass transfer into a turbulent liquid film, Int. J. Heat Mass Tran. 26 (1983) 981–991.

[20] Grossman G., Heath M.T., Simultaneous heat and mass transfer in absorption of gases in turbulent liquid films, Int. J. Heat Mass Tran. 27 (1984) 2365–2376.

[21] Stevanovic V.D., An analytical model for gas absorption in open-channel flow, Int. Comm. Heat Mass Transfer 24 (1997) 1187–1194.

[22] Ghariban N., Haji-Sheikh A., You S.M., Pressure drop and heat transfer in turbulent duct flow: a tow-parameter variational method, J. Heat Trans.-T. ASME 117 (1995) 289–295.

[23] Kays W.M., Turbulent Prandtl Number—where are we? J. Heat Trans.-T. ASME 116 (1994) 284–295.

[24] Zhong Z.Y., Yang K.T., Lloyd J.R., Variable-property natural convection in tilted Enclosures with thermal radiation, in: Lewis R.W., Morgan K. (Eds.), Numerical Methods in Heat Transfer, Vol. III, John Wiley & Sons, Chichester, 1985, Chapter 9.

[25] Patankar S.V., Numerical Heat Transfer and Fluid Flow, Hemisphere/McGraw-Hill, New York, 1980.

[26] Webb B.W., Radiation induced melting of semi-transparent materials, Thesis, Purdue University, August 1986.

[27] Cheremisinoff P.N.P.E., Regino T.C., Principles and Applications of Solar Energy, Ann Arbor Science, Ann Arbor, 1978.

[28] Japanese National Astronomical Observatory (Ed.), Chronological Scientific Tables, Maruzen Co., Ltd., Tokyo, 1994 (in Japanese).